ELSEVIER

Two-dimensional vortex dynamics of inviscid–viscous interaction at turbulent slot-jet impingement

B. M. Tchavdarov
Institute of Mechanics, Bulgarian Academy of Sciences, Sofia, Bulgaria

Turbulent planar jet impinging flows are studied numerically using Chorin's random vortex method. The present study emphasizes inviscid–viscous interaction at the initial stage of impingement on a flat surface as well as on a surface with a shallow cavern of sharp edges. The impinging vortex rebounds from the solid wall, and a secondary vortex is ejected from the viscous layer. Both counter-rotating vortices couple, and as a result of their evolution, a tertiary vortex is formed. The pattern of the inviscid–viscous interaction at impact depends upon the impinged surface (flat surface or surface with a cavern). A search of the literature did not uncover any reference to a turbulent jet impinging on a surface with a cavern of any shape. Comparison with experimental evidence is made for impingement on a flat surface.

Keywords: jet impingement; inviscid–viscous interaction; vortex method

Introduction

In recent years, the recognition that vortex motions are an important feature in the dynamics of the turbulent boundary layer has led to increased interest in understanding the interaction of a vortex with a viscous boundary layer while the vortex approaches a solid boundary. Such an interaction is known as an "inviscid–viscous" interaction. One of the first experimental investigations of an inviscid–viscous interaction is that of Harvey and Perry (1971), who found that a moving vortex could induce eruption from a boundary-layer flow and observed a rebound of the vortex from the wall, which is in apparent contradiction to predictions of the inviscid theory. Fundamental aspects of the inviscid–viscous interaction at impingement were studied experimentally by Didden and Ho (1985). The unsteady boundary-layer flow induced by a vortex approaching a plane wall in a stagnant fluid was investigated by Walker et al. (1987) for a laminar vortex ring and by Peridier et al. (1991) for a two-dimensional (2-D) vortex in the limit problem $Re \to \infty$. In the present study, the inviscid–viscous interaction at 2-D impingement is simulated directly by random vortex method.

Impingement flows are widely observed in many engineering applications because of their high level of momentum and heat transfer. Many papers have been dedicated to theoretical and experimental study of jets impinging on a flat plate. However, in many practical applications, the impinged surface includes confined spaces. For example, in the process of jet cutting, a high-speed jet impacts on a plane surface, but immediately a cavern of sharp edges is formed because of mass removal from the surface. The present investigation includes impingement on a surface with a shallow cavern of sharp edges, as shown in Figure 1.

Turbulent impinging jet flows comprise three regions with different hydrodynamic structures (free jet, stagnation flow, and wall jet), and this makes them a challenging task for physical modeling and numerical simulation. The flow is three-dimensional (3-D), even in the case of symmetric jet nozzles (slot jet and tube jet). However, in the case of slot jet, the large-scale turbulent structures are characterized by 2-D behavior in the jet midplane, and the 2-D theoretical formulation of the problem is reasonable for understanding the slot jet impingement. The impinging jet flows are dominated by localized vorticity distribution in small portions of the flow; namely, in the mixing layers, the stagnation region, and the viscous layer. This makes the vortex methods based on the Lagrangian transport of the vorticity useful and efficient. The advantage of the vortex methods is twofold. First, because the methods are grid free, it avoids the introduction of numerical viscosity, which swamps the physical viscosity in slightly viscous flow. Second, the method is dynamically adaptive: the computational elements participating in the flow naturally cluster in regions of higher vorticity where higher accuracy is required. In vortex methods, there are two different approaches. In the first approach, the vorticity distribution among the particles is reconstructed in each time-step, so that the amount of vorticity carried by each particle is changed under the viscous diffusion effect. Such a solution is deterministic, and the main advantage of this approach is that the number of particles participating in the flow is kept constant. On the other hand, turbulent flows are characterized by local concentration of vorticity that cannot be simulated adequately without clustering a substantial number of particles in these regions of high vorticity. This is achieved by Chorin's random vortex method (see Chorin 1973), which is applied in the present study. In this approach, the

Address reprint requests to Dr. B. M. Tchavdarov, c/o Prof. T. Yabe, Tokyo Institute of Technology, Nagatsuta, Midori-ku, Yokohama 226, Japan.

Received 12 January 1995; accepted 11 July 1996

Int. J. Heat and Fluid Flow 18: 316–327, 1997

655 Avenue of the Americas, New York, NY 10010

0142-727X/97/$17.00
PII S0142-727X(97)00006-4

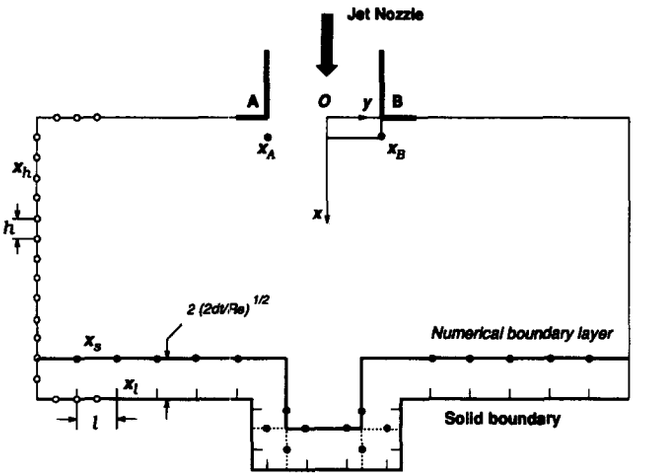

Figure 1 Computational domain, scheme parameters and notations

viscous effects are taken into account by variation of the positions of the particles by means of random walk, and creation of new particles at the solid boundaries. The vorticity carried by each particle is kept constant. The viscous diffusion is simulated by means of Brownian motion of the fluid particles, and the flow as a whole is a stochastic process.

The accuracy of the vortex methods and their ability to resolve small-scale turbulent structures increase with the number of particles N, and this requires implementation of fast algorithms in order to reduce the cost of N-body Biot-Savart calculation of the vortex-induced velocity field. In the present work, we applied the method of local corrections (MLC) introduced by Anderson (1985).

Governing equations and method of solution

The starting equation is the vorticity transport equation in two dimensions; namely,

$$\frac{\partial \omega}{\partial t} = -(\mathbf{u}\cdot\nabla)\omega + \frac{1}{\mathrm{Re}}\nabla^2\omega, \qquad \mathbf{x}\in\Omega; \qquad \mathbf{u}=\mathbf{u}_0 \qquad \mathbf{x}\in\partial\Omega \tag{1}$$

To "close" the above equation, the velocity $\mathbf{u}=(u,v)$ has to be recovered from the vorticity $\omega=\nabla\times\mathbf{u}$. This is achieved by introducing the stream function ψ

$$u=\frac{\partial\psi}{\partial y}, \qquad v=-\frac{\partial\psi}{\partial x} \tag{2}$$

related to the vorticity by the Poisson equation

$$\Delta\psi=-\omega \tag{3}$$

Because in two dimensions, the general solution of the Poisson equation is given by the convolution integral

$$\psi(\mathbf{x},t)=G*\omega=\int G(\mathbf{x}-\mathbf{z})\omega(\mathbf{z})\,d\mathbf{z}, \qquad G=(1/2\pi)\log|\mathbf{x}| \tag{4}$$

we recover the velocity field from the vorticity by

$$\mathbf{u}(\mathbf{x},t)=\int \mathbf{K}(\mathbf{x}-\mathbf{z})\omega(\mathbf{z})\,d\mathbf{z}, \qquad \mathbf{K}=(1/2\pi)(-y,x)/|\mathbf{x}|^2 \tag{5}$$

Following Chorin (1973) the vorticity Equation 1 is split into two parts: one convective and the other diffusion. Let us first consider the convective part, which describes the inviscid flow;

Notation

A, B	nozzle edges
D	nozzle width
f_σ	core function as defined in Equation (11)
H	distance from the nozzle exit to the impinged surface
h	mesh size of the Laplacian grid
L	characteristic length in the wall jet
l	length of a discrete vortex sheet
R	half-width of the nozzle exit
r	radial distance from the jet axes
r_c	correction radius in method of local corrections
r_s	spreading radius in method of local corrections
Re	Reynolds number
S_A	area attached to the nozzle edge A
t	time
U_0	axial velocity at the nozzle exit
U_B	bulk velocity at the nozzle exit
$\mathbf{u}=(u,v)$	velocity vector
$\bar{\mathbf{u}}$	mean velocity
$\mathbf{u}'$	velocity fluctuation
$\mathbf{u}_{\mathrm{pot}}$	potential velocity
$\mathbf{u}_{\mathrm{vor}}$	vortex-induced velocity
$\mathbf{x}=(x,y)$	Cartesian coordinates
z	distance above the impinged surface

Greek

Γ_A	vorticity through the area S_A
δ	Dirac's delta function
$\eta=(\eta_1,\eta_2)$	Gaussian random variables
ν	kinematic viscosity
ξ	sheet intensity
σ	core radius of a vortex blob
ϕ	velocity potential
ψ	stream function
Ω	computational domain
ω	vorticity

Subscripts

0	belongs to an initial or boundary value
A	belongs to nozzle edge A
h	belongs to Laplacian grid
i,j	belong to points of the computational domain
l	sheet stations along the solid boundary
s	blob stations along the outer edge of the numerical boundary layer

i.e., instead of Equation 1 we have

$$\frac{D\omega}{Dt} = 0 \tag{6}$$

where

$$\frac{D}{Dt} = \frac{\partial}{\partial t} + (\mathbf{u}\cdot\nabla)$$

denotes the Lagrangian derivative.

The basic idea behind the vortex methods is to mimic the flow by tracing the fluid particles to which a certain amount of vorticity is associated. This is achieved by a discrete initial value problem derived from Equations 5 and 6 and applying Newton's law of motion. Suppose that a discrete set of particles located at $\mathrm{x}_j \in \Omega$ $(j = 1,2,\ldots,N)$, each of them carrying an amount of vorticity ω_j, approximates at a given time instant t the continuum vorticity field $\omega(\mathrm{x},t)$ in the flow domain Ω; i.e.

$$\omega(\mathrm{x},t) = \sum_{j=1}^{N} \delta(\mathrm{x} - \mathrm{x}_j(t))\omega_j, \qquad \mathrm{x} \in \Omega \tag{7}$$

where δ is Dirac's delta function. Then, from Equations 5 and 7 we arrive at the following problem for the particle's trajectories

$$\frac{\mathrm{d}\mathrm{x}_j}{\mathrm{d}t} = \mathbf{u}_j, \mathbf{u}_j(\mathrm{x}_j(t),t) = \sum_{i=1}^{N} \mathrm{K}(\mathrm{x}_j(t) - \mathrm{x}_j(t))\omega_i,$$

$$t \in [t_0, T]; \qquad \mathrm{x}_j = \mathrm{x}_{j0} \qquad t = t_0 \tag{8}$$

Note, that because of Equation 6, the amounts of vorticity ω_j associated with each particle are constant in time; i.e., $\omega_j = \omega_{j0}$ for $t \in [t_0, T]$. Such a formulated discrete model is singular and produces an extremely large velocity when two particles come close together. The essential numerical idea, introduced by Chorin (1973), is to "smooth" the discretization of the vorticity field (Equation 7) by replacing the point support of vorticity with "smoothed blobs" in order to avoid the singularity in the velocity field. This is done by substituting Dirac's delta function in (Equation 7) with a suitable core function f_σ, σ being a parameter that determines the core of the blob. Hence, instead of Equations 7 and 8 we have, respectively

$$\omega(\mathrm{x},t) = \sum_{j=1}^{N} f_\sigma(\mathrm{x} - \mathrm{x}_j(t))\omega_j, \qquad \mathrm{x} \in \Omega \tag{9}$$

and

$$\frac{\mathrm{d}\mathrm{x}_j}{\mathrm{d}t} = \mathbf{u}_j, \mathbf{u}_j(\mathrm{x}_j(t),t) = \sum_{i=1}^{N} \mathbf{K}_\sigma(\mathrm{x}_j(t) - \mathrm{x}_j(t))\omega_i,$$

$$t \in [t_0, T]; \qquad \mathrm{x}_j = \mathrm{x}_{j0} \qquad t = t_0 \tag{10}$$

where $\mathbf{K}_\sigma = \mathbf{K} * f_\sigma$. The approximation function $f_\sigma(\mathrm{x} - \mathrm{x}_j)\omega_j$ is called "vortex blob." In our analysis, we use the core function originally introduced by Chorin (1973), which sets the radial velocity inside a given cut-off size σ to be constant; namely,

$$f_\sigma(|\mathrm{x}|) = \frac{1}{2\pi\sigma|\mathrm{x}|}, \qquad \text{for} \qquad |\mathrm{x}| \le \sigma \qquad \text{and}$$

$$f_\sigma(|\mathrm{x}|) = 0, \qquad \text{for} \qquad |\mathrm{x}| > \sigma \tag{11}$$

The above choice of $f_\sigma(r)$ gives the following expressions for the smoothed kernel:

$$\mathbf{K}_\sigma = \begin{cases} (-y,x)/2\pi|\mathrm{x}|\sigma & |\mathrm{x}| < \sigma \\ (-y,x)/2\pi|\mathrm{x}|^2 & |\mathrm{x}| \ge \sigma \end{cases}$$

The viscous diffusion is simulated by allowing the vortex element to undergo a random walk. Thus, the correction to the blob's locations x_j due to diffusion for the time increment Δt is added as a random step $\eta = (\eta_1, \eta_2)$, where $\eta_{1,2}$ are Gaussian random variables with zero mean and variance $2\Delta t/\mathrm{Re}$.

Boundary conditions, vorticity creation, and numerical algorithm

An essential part of the algorithm is the treatment of the boundary conditions, their effect on the potential flow, on viscous diffusion, and on vorticity creation. The computational domain of the flow is shown in Figure 1. In the finite domain, the general solution of the homogeneous Equation 3 with uniform zero vorticity differs from the trivial one. Hence, the potential velocity field has to be resolved and added to the vortex-induced velocity, as obtained by Bio-Savart calculations in Equation 10. Finally, the new positions of the particles are given by

$$\mathrm{x}^{n+1} = \mathrm{x}^n + \Delta t\left(\frac{3}{2}\mathbf{u}^n - \frac{1}{2}\mathbf{u}^{n-1}\right) + \eta,$$

$$\mathbf{u} = \mathbf{u}_{\mathrm{pot}} + \mathbf{u}_{\mathrm{vor}}, \qquad \eta = (\eta_1, \eta_2) \tag{12}$$

where $\mathbf{u}_{\mathrm{pot}}$ and $\mathbf{u}_{\mathrm{vor}}$ are the potential velocity and vortex induced velocity, respectively, and η is a random walk. Note, that resolving the potential velocity requires the Laplace equation for the potential function ϕ, $\mathbf{u} = \nabla\phi$

$$\nabla^2\phi = 0, \qquad \mathrm{x} \in \Omega \tag{13}$$

to be solved at each time-step because of time-dependent Neuman boundary conditions

$$\frac{\partial\phi}{\partial\mathbf{n}} = (\mathbf{u}_0 - \mathbf{u}_{\mathrm{vor}})\cdot\mathbf{n} = 0, \qquad \text{on} \qquad \partial\Omega \tag{14}$$

where $\mathbf{u}_0$ is the prescribed velocity at the boundaries (zero at solid boundaries and inlet/outlet velocity at nozzle/outlet boundaries); $\mathbf{u}_{\mathrm{vor}}$ is vortex induced velocity at the boundary which depends on time; $\mathbf{n}$ is the outer unit normal vector.

The above algorithm requires particle-to-particle (PP) Bio-Savart calculations for the vortex-induced velocity, which enormously increase the cost of computations for number of particles on the order 10^4 or more. One way to reduce the computational time is to remain in the frame of PP force calculation scheme but to combine a cluster of vortices in one computational element; for example, the fast multipole method (FMM) of Greengard and Rockhin (1987) based on the multipole expansion or the hierarchical element method (HELM) of Anderson (1992) based on Poisson's formula for the velocity potential. Another approach is to take advantage of the lower computational cost of the Poisson Equation 3 far from the computational point and, at the same time, to preserve the higher accuracy of the PP calculation scheme near the computational point. This is achieved by particle-particle-particle-mesh (PPPM) methods. In the case of a

complex computational domain, we must solve the field equation on a Laplacian grid at each time-step at least to resolve the potential velocity component, regardless of the fast summation techniques applied. In the PPPM methods, the far-field vortex-induced velocity and potential velocity are obtained at the same time by solving the Poisson equation, and their application requires fewer additional programming codes, as compared to FMM or HELM. Both approaches reduce the computational cost from $O(N^2)$ to the order of $O(N \log N)$. The main problem in PPPM methods is how to preserve the high accuracy of the PP scheme and to avoid the scheme viscosity due to introduction of the Laplacian grid in the calculation of far-field vortex-induced velocity. This is achieved by the method of local corrections (MLC), which we prefer in the present work. The MLC uses the following steps.

1. Compute the velocity field $\mathbf{u}_h$ induced by the vortices onto the grid points of the Laplacian grid Ω_h as if these vortices were point vortices (velocity summation formula as in Equation 8).
2. Define a discrete Laplacian g_h^{Ω} on Ω_h, in such a way that g_h^{Ω} is exactly $\Delta^h \mathbf{u}_h$ *near* the vortex but is set to zero *far from* the vortex.
3. Modify the grid velocity $\mathbf{u}_h$ by solving the Poisson equation

$$\Delta^h \tilde{\mathbf{u}} = g_h^{\Omega} \tag{15}$$

under the boundary conditions of Equation 14.

4. Correct locally the grid velocity $\tilde{\mathbf{u}}$, and interpolate onto the vortices accounting for the "smooth" interaction between *nearby* vortices (velocity summation formula as in Equation 10).

To determine which vortices are *near to* and which are *far from* a given vortex, we apply a link-list technique, as described by Hockney and Eastwood (1981).

The MLC is an essential modification to the particle-particle-particle-mesh method (PPPM) in that it allows for the fact that the velocity field induced by a point vortex is harmonic away from its center. For more details on MLC see Anderson (1985) and Almgren et al. (1994). An extensive review of the recent advances in fast multipole methods (FMM) is given in Strickland and Baty (1995).

The second aspect of the numerical algorithm concerns treatment of the viscous boundary layer near the solid boundaries. Along the solid boundaries, in a thin numerical boundary layer we apply a vortex sheet algorithm (Chorin 1978; 1980) according to the Prandtl boundary-layer approximation of the vorticity Equation 1. The vorticity inside the layer is discretized by vortex sheets of finite length that interact in accordance to a prescribed force law.

Until now, we have supposed the vortex elements (blobs inside the domain and sheets in the viscous boundary layer) initially approximate the continuum distributed vorticity in the flow domain. This cannot be achieved without correct generation of new discrete vortex elements from the solid boundaries (the nozzle edges and the impinged surfaces), where the vorticity initially is created from zero. It should be noted that in 2-D modeling, the local enhancement of vorticity is solely attributable to shear, and it is accomplished numerically by clustering of the vortex elements by means of convection and diffusion. This is in contrast to the 3-D approach where the enhancement of vorticity is also attributable to "straining," which is simulated by vortex tube stretching mechanism.

The vortex elements that enter the flow from the impinged surfaces are vortex sheets. The latter are generated in such a way that the nonslip boundary condition $(\tilde{\mathbf{u}} \cdot \tau) = 0$ is satisfied at each time-step. The jump in tangential velocity across the sheet determines its strength. It requires discrete vortex sheets of total strength $(-\tilde{\mathbf{u}} \cdot \tau)$ to be located along the solid boundary. These vortex sheets initially enter the flow domain by a random walk in the normal direction to the boundary (in the Prandtl boundary-layer approximation diffusion is neglected in the tangential direction).

The inlet vorticity is generated from the nozzle edges. The total vorticity (more precisely, the total circulation) that we assign to the vortex blobs entering the flow from edge B (see Figure 1) is approximated as follows.

Let $U_0 = \max_y u_0(y)$ be the maximum velocity at the nozzle exit. Near the nozzle, at a distance $\Delta t U_0$, we can assume $v \equiv 0$, so that $\omega \equiv du_o/dy$ in the thin area below the nozzle, $S_B = (\Delta t U_0) \times R$, R being the nozzle half-width. If we denote Γ_B the total vorticity through the area S_B then

$$\Gamma_B = \int\int_{S_B} \omega \, dx \, dy = \Delta t \int_0^R (u_0 \omega) \, dy$$

$$= \Delta t \int_0^R \left(u_0 \frac{du_0}{dy} \right) dy = -\frac{\Delta t}{2} U_0^2$$

Respectively, the vorticity generated from the nozzle edge A will be $\Gamma_A = (\Delta t/2) U_0^2$. The total amount of vorticity Γ_A is distributed among n blobs entering the flow from the point $\mathbf{x}_A = (-R, \Delta t U_0)$. The same number of blobs will carry out the vorticity generated from the point $\mathbf{x}_B = (R, \Delta t U_0)$.

Parameters selection and sensitivity of the computations

As scaling parameters, we chose the nozzle width D and the axial value of the jet exit velocity U_0. The nondimensional parameters of the problem are the Reynolds number $\mathrm{Re} = DU_0/\nu$, the stand-off distance H/D, measured along the centerline from the nozzle exit to the impinged surface, and the dimensions of the cavern, if the latter is present.

Implementation of the Random Vortex Method requires a proper choice of a number of scheme parameters. The main parameters are the time step Δt, the sheet length l, and the maximum sheet intensity $\xi_{\max}$. Two stability conditions have to be satisfied (see Puckett 1991): $\Delta t U_0 \le l$ and $\Delta t \xi_{\max} \le l^2/L$, where L is a characteristic length in the wall jet. The impinged surface is discretized uniformly by a local panel length l. Dummy boundary sheet probes $\mathbf{x}_l$ are located at the boundary nodes (see Figure 1). At each time-step, vortex sheets of strength no greater than $\xi_{\max}$ enter the flow from a sheet probe $\mathbf{x}_l$ in order to annihilate the tangential velocity $(\mathbf{u}(\mathbf{x}_l) \cdot \tau)$. The same velocity is taken as a sky velocity at dummy probes $\mathbf{x}_s$ for the numerical boundary layer of thickness equal to $2 \times$ (standard deviation) $= 2(2\Delta t/\mathrm{Re})^{1/2}$.

The algorithm of sheet interaction inside the numerical boundary layer, and sheets/blobs trade at the outer edge of the layer is organized as in Sethian et al. (1992). A unit vector pointing in the inward normal direction of the corresponding wall is attached to each sheet so that the sheets that belong to different solid walls do not interact with each other. From the matching conditions at the boundary-layer edge: i.e., continuity of vorticity carried by the vortex element and continuity of the induced tangential velocity at the solid boundary, we get, respectively, the intensity of the vortex blob $\omega = l\xi$ and the core radius $\sigma = l/(2\pi)$.

The MLC requires the computational domain to be covered by a Laplacian grid Ω_h of mesh size h. The normal component of the vortex-induced velocity necessary for the boundary condition (Equation 12) is computed at the dummy boundary blob probes located at the grid boundary nodes $\mathbf{x}_h$. The chosen spreading distance r_s and the correction radius r_c in the MLC

algorithm are $r_s = r_c = 2h$ (Anderson 1985). An auxiliary "chaining mesh" $\Omega_k \subset \Omega_h$ of mesh width $k = 2h$ is used for the link-listing technique. Each vortex blob is assigned a tag to indicate to which grid box of the chaining mesh the vortex belongs. The blobs are sorted, and all vortices with the same tag are linked together. The link-listing technique substantially reduces the number of operations required to determine which blobs are near to and which are far from a given vortex blob.

The random vortex method views the solutions of the Navier–Stokes equations as random fields, and what we obtain in the numerical experiment is a sample of a random field. To get the mean flow characteristics and fluctuating quantities at a prescribed point in space, we must have the history of the numerical solution (blobs' locations and their strengths) over a large enough time interval. Then, a dummy vortex blob is located at that point, and by a second "fast run" of the flow history, we get the time-averages of the mean and fluctuating quantities at the prescribed point. The mean velocity $\bar{\mathbf{u}}$, the rms of turbulent velocity $\mathbf{u}' = \mathbf{u} - \bar{\mathbf{u}}$ and the rms of turbulent shear stress $u'v'$ are taken over 50 time units in a fully developed turbulent flow. Numerical convergence of the results is clearly manifested by increasing the time interval. In the wall jet, the solution at a distance $r = y_1$ from the jet axes is obtained as an averaged solution at normal cross sections $y = y_1$ and $y = -y_1$. In the present study, after some numerical experimentation, we chose the following values for the scheme parameters: $\Delta t = 0.1$, $l = 0.2$, (core radius $\sigma = 0.016$) $\xi_{max} = 0.1$, $h = 0.15$.

With the above scheme parameters, the number of the vortex elements in the end of computations and the mesh points of the Laplacian grid vary between experiments in the following limits: 40,000 blobs; 15,000 sheets; and 10,000 mesh points. For the case $H/D = 6.0$ and a length of the impinged wall equal to $24D$, there are 22,223 blobs and 835 sheets in the computational domain at $t = 40$. This example runs 2 hours, 23 minutes on Silicon Graphics Indigo with application of MLC algorithm. A comparison with a direct M-body computations shows that MLC technique reduces the computational time 4.3 times, while the relative error in the streamwise mean velocity is less than 2.5%.

With refinement of the scheme parameters, we observe the following in a series of numerical experiments: 1) the large-scale vortex dynamics and the global eddy quantities, such as shape, size, and velocity remain unchanged; 2) local numerical convergence in the time-averaged mean velocities; 3) the maximum difference in the time-averaged fluctuating velocity remains in the limit of 10% in the stagnation region and 15% in the wall jet; however, a pointwise numerical convergence of the time-averaged fluctuating velocity was not clearly observed when increasing the number of vortex elements up to 50,000; and 4) the numerical results are most sensitive to the number of vortex elements controlled by the maximum intensity ξ_{max} and less sensitive to the time-step and space discretization parameters.

It should be noted that the numerical boundaries downstream of the wall jet are a source of error for the solution in the interior, because the vortex elements do not interact with those elements that are supposed to exist behind the numerical boundaries. It is difficult to estimate the distance where this boundary error spreads with time, but to ensure correct results for a fully developed wall jet, we should disregard the solution at least one characteristic length inside the numerical boundary.

Numerical results and discussions

For validation of the numerical method, quantitative results in the case of a fully developed turbulent impingement on a flat surface are presented in Figures 2–5 as compared with the experimental data for planar jet of Saad et al. (1992) and Kumada et al. (1973) and with the experimental data for round jets

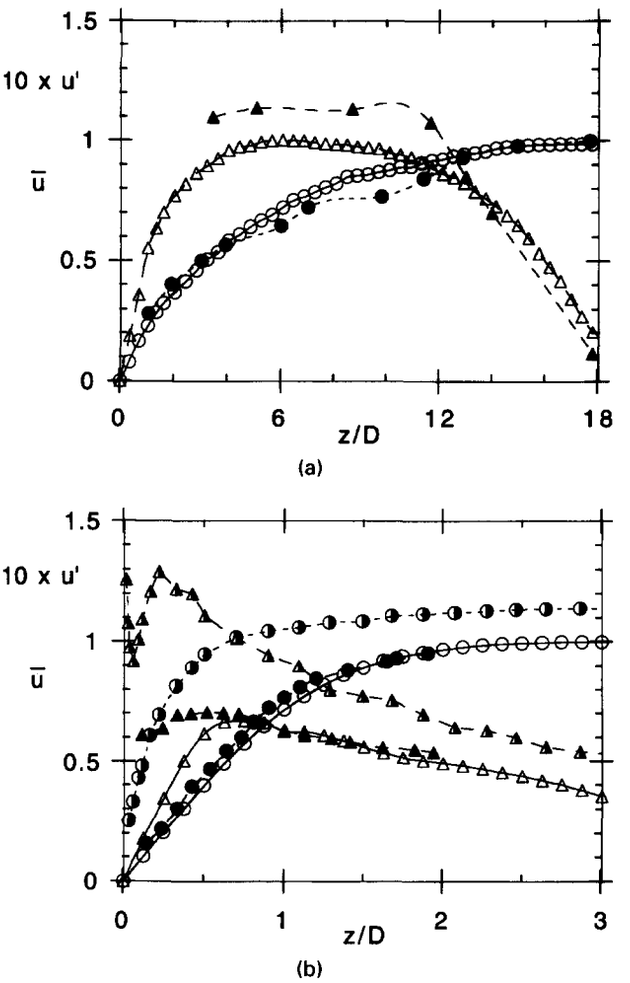

Figure 2 Mean axial velocity and rms turbulent velocity on the stagnation line as compared with the experimental data; ○-mean velocity; Δ-turbulent velocity; (a) $H/D = 19$, Re = 11,000; open symbols, the present 2-D analysis; filled symbols, experimental data for a slot jet, Saad et al. (1992); (b) $H/D = 6$, open symbols, the present 2-D analysis, Re = 23,000; filled symbols, experimental data for slot jet, Kumada et al. (1973), Reynolds number is in order of 10^4; half-filled symbols, experimental data for round jet, Cooper et al. (1993), Re = 23,000

of Craft et al. (1993) and Cooper et al. (1993). The comparison between 2-D modeling of slot jet impingement and experimental data for round jet impingement is mostly qualitative, and it has been included to show the effect of vortex stretching mechanism —the latter being neglected in 2-D analysis while playing a significant role in 3-D round jet impingement.

The normal mean velocity and the corresponding rms of the velocity fluctuations along the jet axis are plotted in Figure 2. The distance from the wall is denoted by z/D. The centerline exit velocity U_0 is used as a scale in the case of a slot jet impingement, while the experimental data for the round jet are normalized by the bulk exit velocity U_B. The predicted mean velocity agrees well with the experiment for slot jet impingement all over the jet axis. The comparison between the corresponding turbulent velocities is good far from the wall, where it is determined by a diffusion of turbulence from the mixing region. Near the stagnation point, the present simulation predicts a lower level of turbulent fluctuations, as can be seen in Figures 3 and 4, as

compared with a round jet. This probably is attributable to the 3-D character of turbulence in the stagnation region—strongly manifested in the laboratory experiment with round jets and less so in the case of slot jets.

In both examples (Figures 2a and b) the drop in the predicted axial mean velocity profile starts about $0.3H$ from the wall, which is a larger value than the corresponding distance observed for a round jet by Cooper et al. (1993). This probably is due to the higher spreading rate in the case of 2-D slot jet [the measured spreading rate for plane jet is 0.110 as opposed to 0.093 for round jet, Launder (1989)] accompanied by correspondingly higher shear stress levels. As seen in Figure 5c, a significant increase in the turbulent shear stress level is predicted at about the same distance: i.e., $0.3H$ from the wall.

The turbulent fluctuations in the wall jet shown in Figures 3–5 compare with those of the round jet data. The predicted velocity profiles parallel to the wall exhibit the same order of magnitude and a pattern similar to those observed in the experiments for round jets of Craft et al. (1993), with more pronounced differences near the stagnation line. The level of the fluctuations normal to wall, as predicted by the present analysis, is less than that observed in the case of a round jet. A comparison between the predicted fluctuations of the velocity normal to wall (u-component) and those parallel to wall (v-component) shows the wall effect of "redistribution" in velocity fluctuations from normal to streamwise (parallel to wall) direction, which results in a reduction of the turbulent shear stress. This is shown clearly in Figure 5.

The present analysis aims to predict the mechanism of inviscid–viscous interaction at the initial stage of turbulent impingement. The evolution of the vortex dynamics at impingement on a flat surface is shown in Figure 6. The dots indicate the locations of the vortex blobs, and the arrows point the directions of the velocity vector. The length of the arrows is half of the magnitude of velocity. From the beginning of the computations, to the time instant $t = 23$ (not shown in the figure), the primary vortex pair, generated from the nozzle edges, was approaching the wall, while a fully turbulent boundary layer has been developed along the wall by vortex blobs, entering the flow from the numerical boundary layer, when the vortex sheets crossed the boundary-layer edge. In the first image (Figure 6a), the primary vortex impacts on the wall, which causes a thickening of the boundary layer slightly downstream of the vortex core. This thickening of the boundary layer is accompanied by induction of an intense vorticity layer that is unstable and rolls up, forming a secondary vortex. This process is shown clearly in Figures 6a and b as an eruption from the boundary layer. The primary and second vortices move downstream along the wall in a counter-rotating pair. Because of the higher circulation of the primary vortex, the

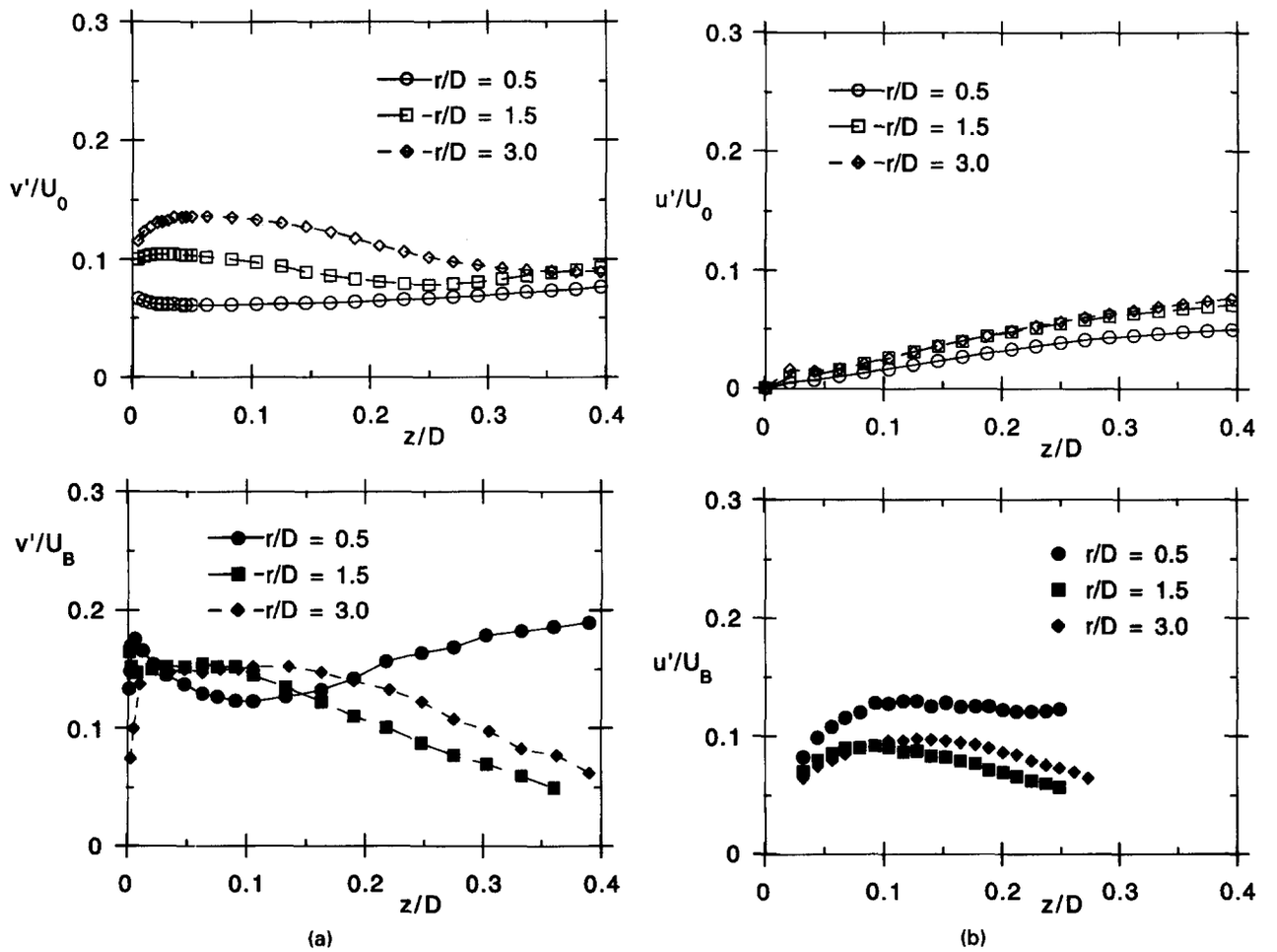

Figure 3 Profiles of rms turbulent velocity in radial wall jet; $H/D = 6$, Re = 70,000; (a) component parallel to wall; (b) component normal to wall; open symbols, the present 2-D analysis; filled symbols, experimental data for a round jet, Craft et al. (1993)

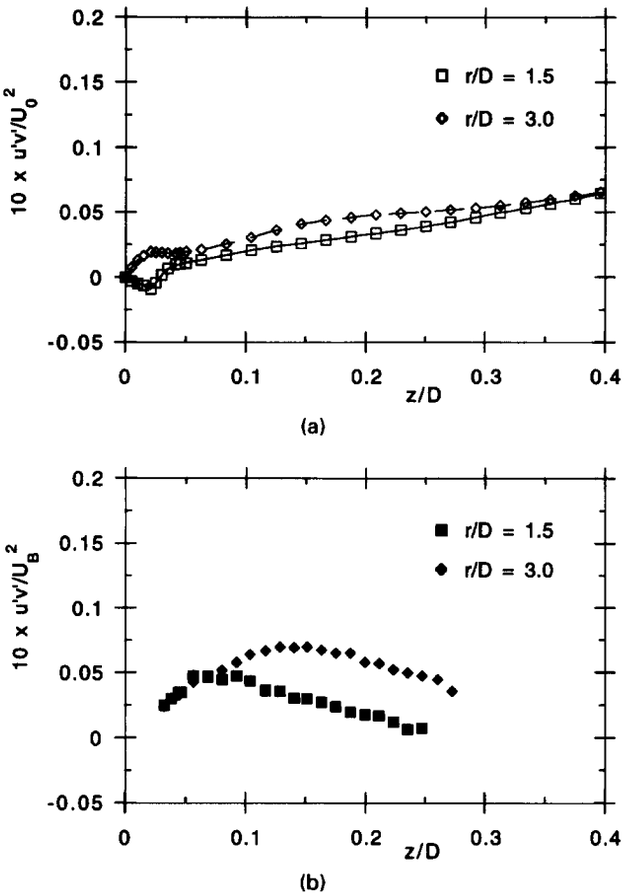

Figure 4 Profiles of rms turbulent shear stress in radial wall jet; $H/D=6$, Re=70,000; (a) present 2-D analysis; (b) experimental data for a round jet, Craft et al. (1993)

secondary vortex lifts off the wall (Figure 6d) and finally is wrapped around the primary vortex (Figure 6e). Both vortices move along a curve trajectory concave in the direction of the primary vortex. As a result of the rolling of the vortex pair above the boundary layer, a second eruption occurs, caused by the primary vortex, and a tertiary vortex is ejected from the viscous layer (see Figure 6e). Finally, the secondary and the tertiary vortices reach strength and dimension compatible with the primary vortex. A schematic diagram of the ejection of secondary and tertiary vortices in the case of impingement on a flat plate is shown in Figure 7.

The vortex dynamics in the example above exhibits the main features of the inviscid–viscous interaction observed experimentally in the pioneering work of Harvey and Perry (1971) on the evolution of aircraft trailing vortices influenced by the ground. The present results also agree qualitatively with the experimental and theoretical investigations of Walker et al. (1987) for the impact of a vortex ring on a wall; although, in purely 2-D flows, as is the case in the present study, the vortex dynamics are free of vortex-stretching mechanism.

In many cases, the process of inviscid–viscous interaction is accompanied by a separation of the boundary layer from the wall. In impinging jets, an unsteady separation in the wall jet is induced by the primary vortex, and a separation point moves downstream in the radial mean flow direction. This aspect of the inviscid–viscous interaction is studied experimentally in detail by Didden and Ho (1985) for axisymmetrical impinging jets and theoretically by Peridier et al. (1991) for a 2-D vortex approach-

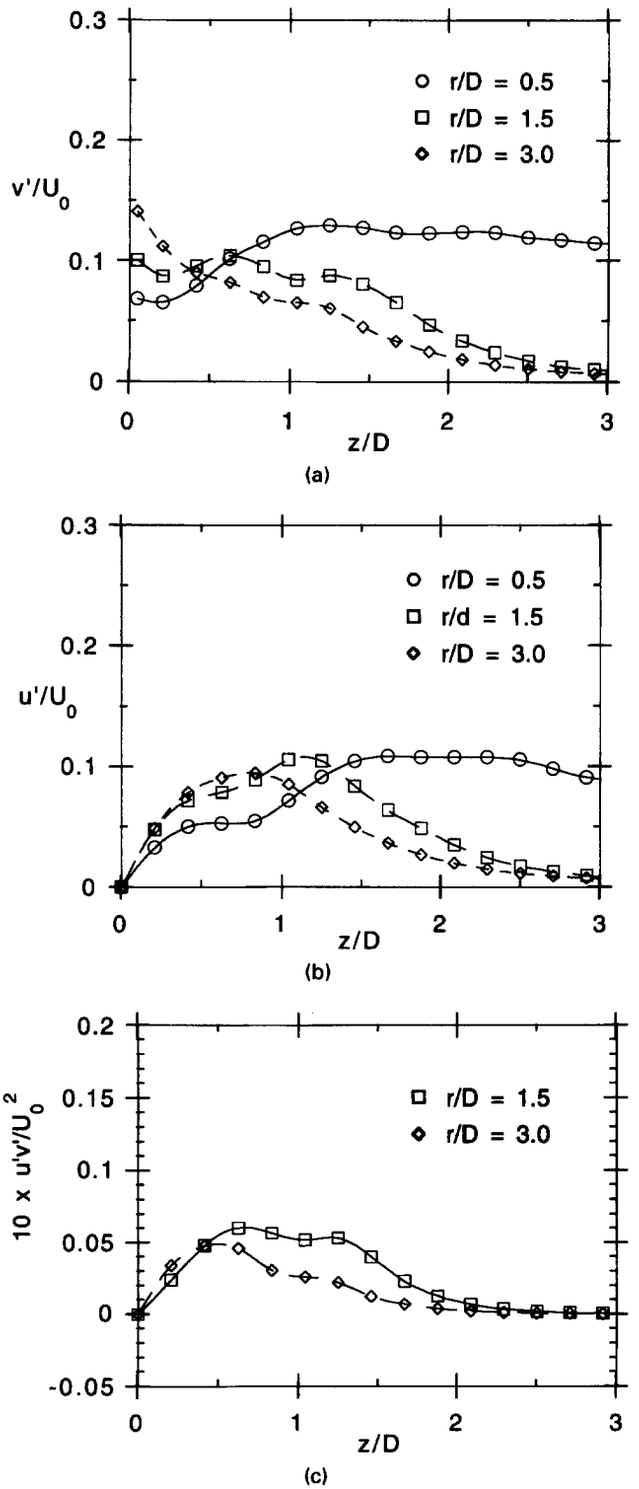

Figure 5 Extended profiles of rms turbulent velocity and shear stress in the radial wall jet as predicted by the present 2-D analysis for slot jet impingement; $H/D=6$, Re=70,000; (a) velocity component parallel to wall; (b) velocity component normal to wall; (c) turbulent shear stress

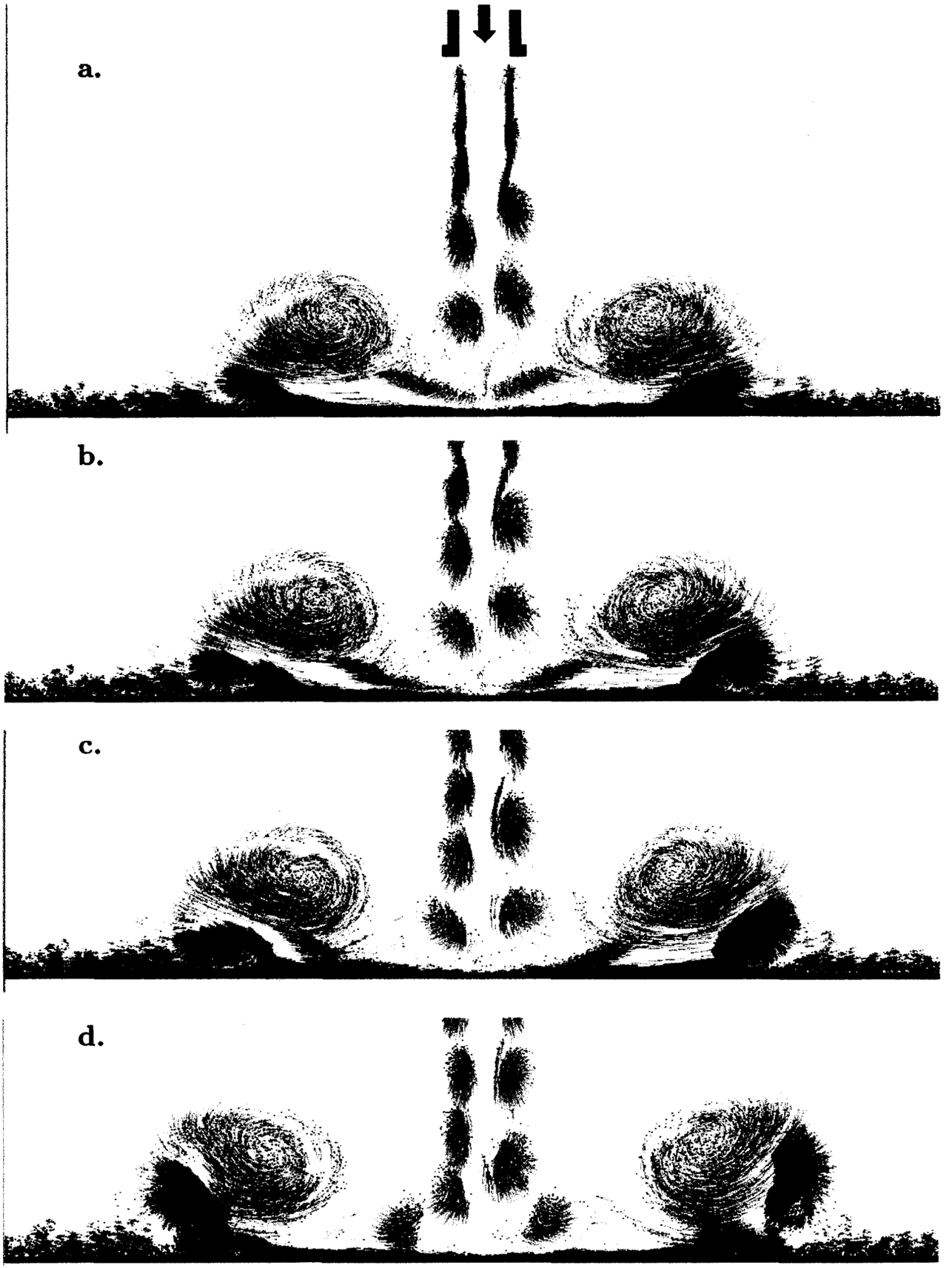

Figure 6 Vortex dynamics of impinging jet on a flat surface; Re=23,000, $H/D=7$; (a) $t=26$; (b) $t=27$; (c) $t=28$; (d) $t=30$; (e) $t=33$; (f) $t=39$

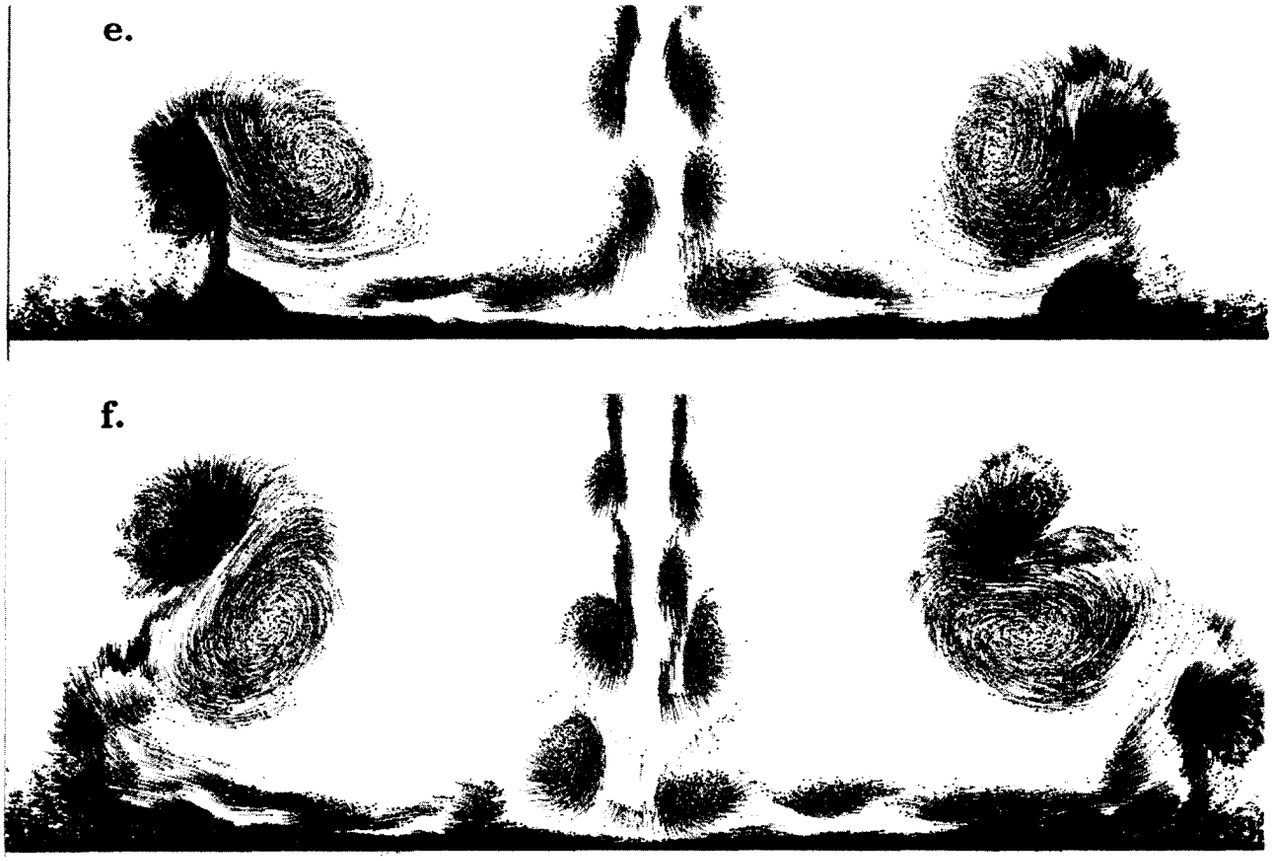

Figure 6 (Continued)

ing a plane wall in the limit problem Re → ∞. The random vortex method applied in the present study is based on the Prandtl boundary-layer equations, which causes difficulties in prediction of the boundary-layer separation where a well-defined boundary-layer region fails to exist. However, the symptoms of an unsteady separation; namely, the thickening of the boundary layer and the ejection of the vorticity are clearly manifested by the random vortex method.

Vortex dynamics of an inviscid–viscous interaction at the initial stage of impingement on a surface with a shallow cavern of sharp edges is shown in Figure 8 and schematically depicted in Figure 9. The primary vortex approaches the cavern and impinges on its leading edge. As a result of a strong interaction with the viscous layer, the primary vortex is arrested at the edge and immediately rebounds from the wall at a large angle of approximately 40° (Figure 8b, c). At the time of impact, a rapid thickening of the boundary layer is observed at the leading edge of the cavern, and an eruption of vorticity as a secondary vortex results from the inviscid–viscous interaction (Figure 8a, b). The secondary vortex is entrained in the motion of the primary vortex, and the counter-rotating couple moves away from the wall. For a short time, the secondary vortex remains connected to the edge of the cavern by vortex sheet, as shown in Figure 8c. This vortex sheet is unstable and in some cases transforms into a tertiary circular vortex (Figure 8d, e, left vortex pair). When the primary vortex impacts on the leading edge of the cavern, the vortex tail breaks, and a part of it interacts with the local boundary layer inside the cavern. As a result, small recirculation zones are formed in the bottom corners of the cavern. It should be noted that the dimensions of the cavern are chosen in such a way that the primary vortex pair impinge on its edges, as is the case of the initial phase of the jet-cutting process. The case of impingement in a deep cavern exhibits a completely different pattern of vortex dynamics, which is beyond the scope of the present study.

Conclusions

The random vortex method has been applied to direct simulation of turbulent 2-D impinging jet flows. The method considers the solution of the Navier–Stokes equations as being random field (Chorin 1994). Such an approach is plausible both theoretically and experimentally: for large Reynolds numbers, the flow described by the Navier–Stokes equations is chaotic; in the laboratory test, there are no two identical experiments, and what we observe is a function of the experiment. The method is free of artificial viscosity, and it is even more accurate for high Reynolds number, in contrast to the grid methods, where the artificial numerical viscosity increases with the increasing Reynolds num-

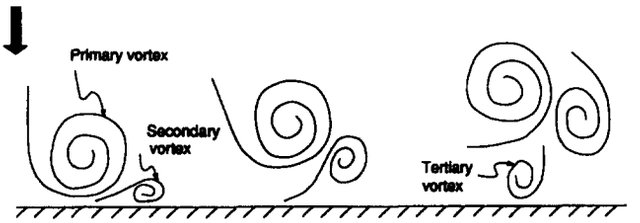

Figure 7 Schematic diagram of inviscid–viscous interaction at impingement on a flat surface; secondary and tertiary vortices are ejected from the boundary layer

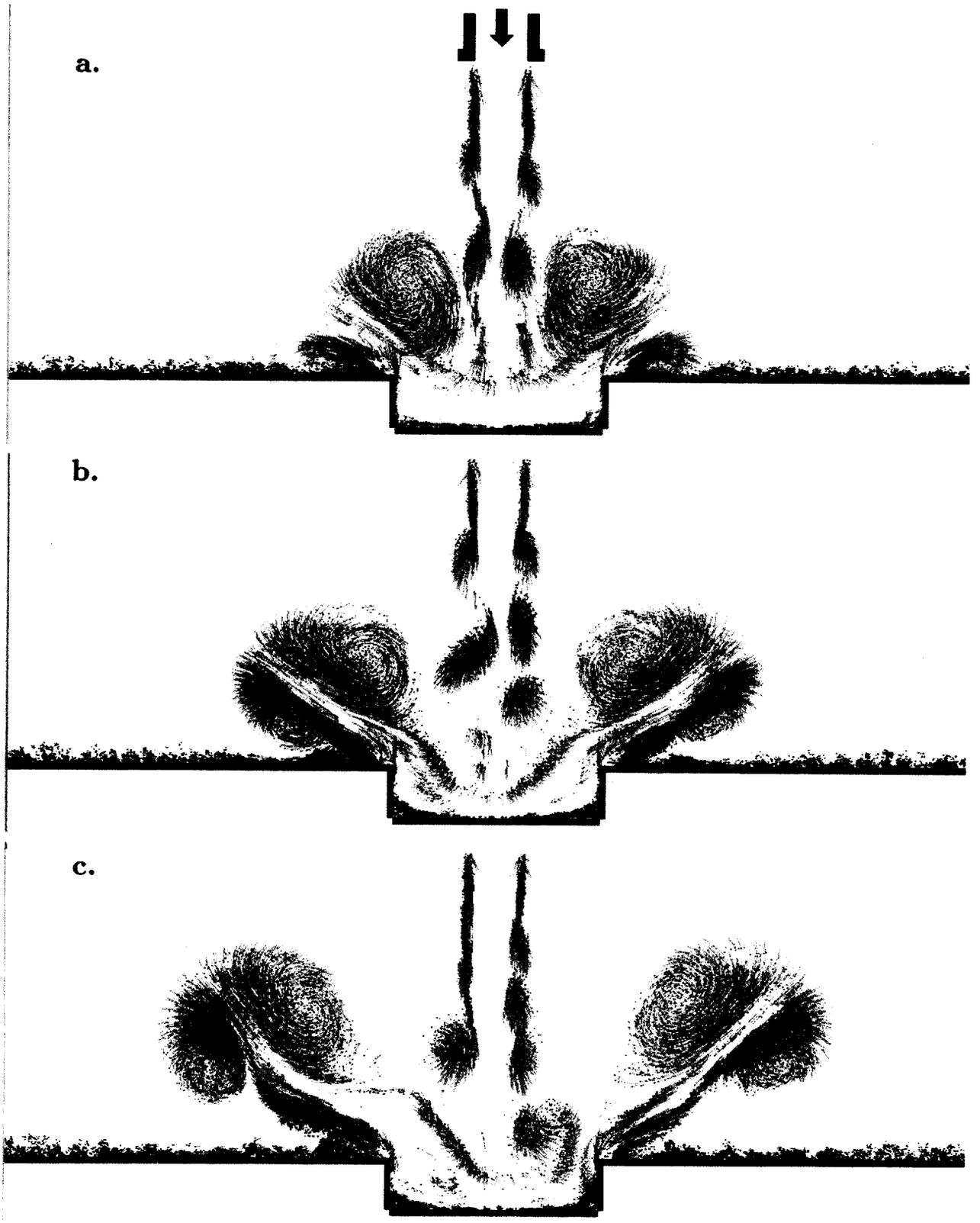

Figure 8 Vortex dynamics of impinging jet on a surface with a shallow rectangular cavern of sharp edges; Re=23,000, $H/D=7$; dimensions of the cavern: width=4 D; depth=D; (a) $t=20$; (b) $t=24$; (c) $t=28$; (d) $t=32$; (e) $t=34$

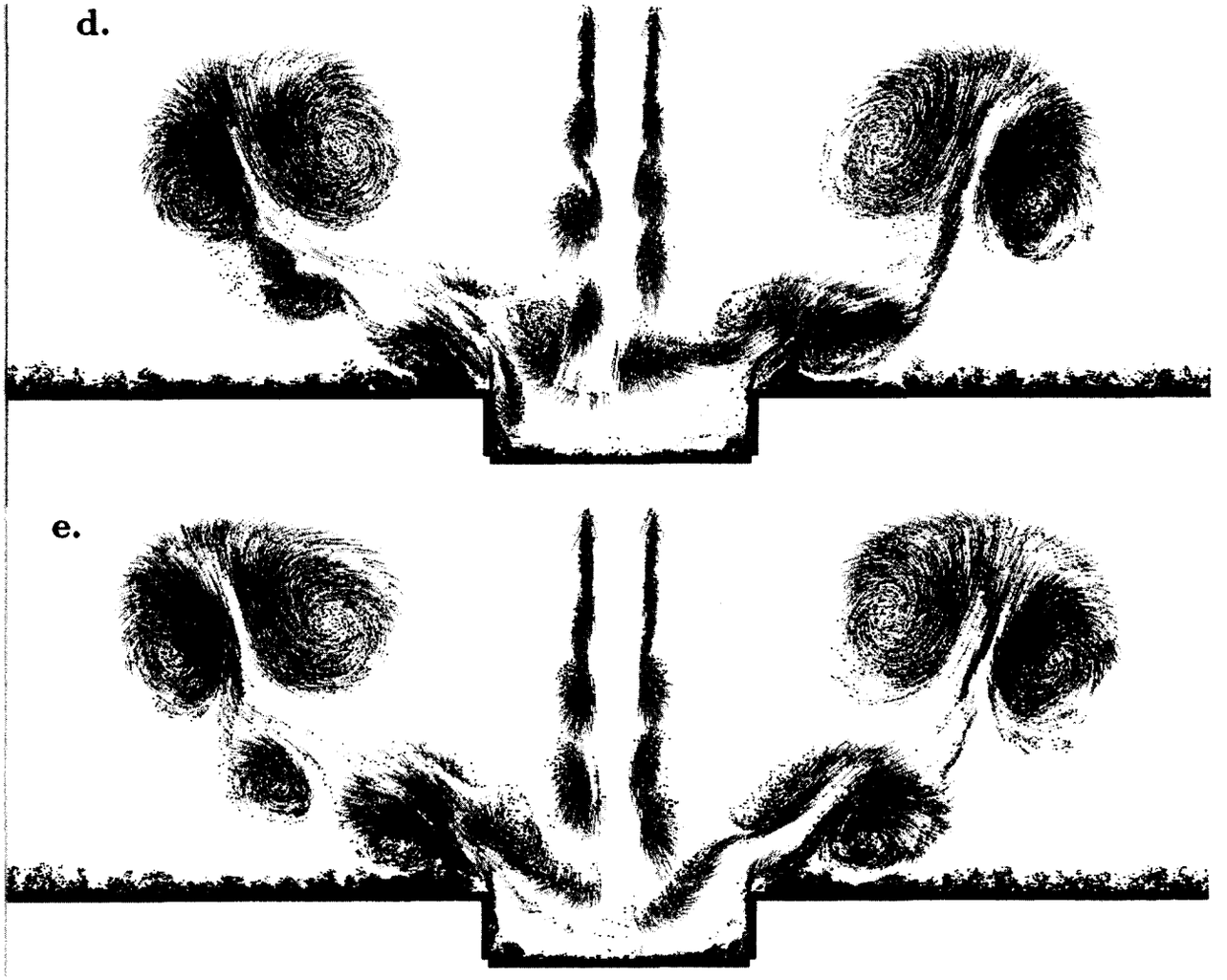

Figure 8 (Continued)

ber. Numerical tests on the convergence and accuracy of the results show: 1) the mechanism of the inviscid–viscous interaction at impingement, as well as large-scale global quantities, can be predicted with a relatively small number of vortex elements (20,000–30,000); and 2) with increasing vortex elements, the turbulent fluctuations decrease but remain above a certain level; however, local numerical convergence in the fluctuations was not clearly observed with as many as 50,000 vortex blobs. Analysis of a fully developed turbulent impingement requires many hours of computational time, and it is not reasonable without an application of the fast summation algorithm.

An important aspect of numerical modeling of turbulent impingement flows is the treatment of viscous diffusion near the impinged surface. The random vortex method utilizes vortex sheets in a thin numerical layer along the solid boundaries. The vortex sheet algorithm assumes a well-defined Prandtl boundary layer in the vicinity along the wall (which does not exist near the stagnation point) as well as near the unsteady separation point in the turbulent wall jet. Another source of error related to the vortex sheet algorithm is the matching conditions with outer solution (sheet–blob exchange). This error seems to be dominant in the boundary-layer approximation. Recently, a new diffusion scheme for vortex methods was proposed by Strickland et al. (1995), and a comparative study will be a useful future investigation.

The present study emphasizes the inviscid–viscous interaction at the initial stage of impingement. Computations on a flat surface reveal the main features of the phenomenon that agree qualitatively with the experimental evidence. The impinging primary vortex ejects secondary and tertiary vortices from the

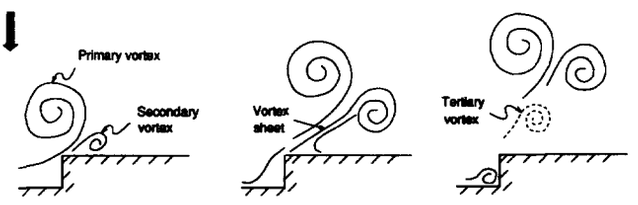

Figure 9 Schematic diagram of inviscid–viscous interaction at impingement on a surface with a rectangular cavern of sharp edges; a secondary vortex is ejected from the boundary layer immediately after the leading edge, and a vortex sheet is formed in between; this vortex sheet is unstable, and, in some cases, it is transformed to a tertiary vortex

boundary layer, and thus, the vorticity protrudes into the inviscid region. In the case of impingement on a surface with a shallow, sharp-edged cavern, a strong rebound of the primary vortex is observed, while the latter impinges on the leading edge of the cavern. Simultaneously, a strong eruption from the boundary layer, immediately downstream from the leading edge, forms a secondary vortex that couples with the primary vortex. In contrast to the impingement on a flat surface, the primary vortex interacts with a small region of the boundary layer; namely, the leading edge of the cavern, and the tertiary vortex is not ejected from the layer at the initial phase of impingement; however, in some cases, it is formed from the vortex sheet between the leading edge of the cavern and the secondary vortex. Even in the presence of a very shallow cavern in the impinged surface, the inviscid–viscous interaction at turbulent impingement is strongly influenced by the cavern.

It should be emphasized that all the results in the present paper were obtained by pure 2-D modeling of turbulence, which is only an approximation of reality. In 2-D modeling, vortex dynamics are governed by convection and viscous diffusion, while they do not account for the vortex-stretching mechanism. The latter has a significant effect on the vortex dynamics in 3-D structures. Turbulent flows involve many scales of motion that are strongly coupled. The small-scale motions are always 3-D structures. Then, how valid are 2-D computations for turbulent flows? This question is still open. To our knowledge, there is no systematic exploration of the usefulness of 2-D computations of turbulent flows. If the geometry of the flow domain is essentially 2-D, the motion in the largest scale can be assumed to be 2-D also, if the flow is not dominated by the effects of a turbulent boundary layer. The present 2-D computations on a flat surface qualitatively predict the main features of the inviscid–viscous interaction at slot jet impingement, and the quantitative analysis supports the experimental observations. This leads us to believe that the present 2-D computations are a good approximation of reality.

Acknowledgments

The author is grateful to Alexandre Chorin, University of California, Berkeley, for his help on the numerical method and for many useful discussions. The author also thanks his colleagues from Kajima Technical Research Institute, Japan, where this research was performed. I am grateful to Dr. Yoshida and Dr. Isobe for their financial support and to Dr. Horikoshi, Mrs. Nakayama, Mrs. Yano, and Mrs. Shimada for their help with visualization and graphics. This research was supported by Kajima Technical Research Institute, Japan, during the author's term as a Visiting Researcher. It was also partially supported by the European Community during a short-term fellowship in the Mathematical Institute of Oxford University.

References

Almgren, S. A., Buttke, T. and Colella, P., 1994. A fast adaptive vortex method in three dimensions. *J. Comp. Physics*, **113,** 177–200

Anderson, C. 1985. A method of local corrections for computing the velocity field due to a distribution of vortex blobs. *J. Comp. Phys.*, **62,** 111–123

Anderson, C. 1992. An implementation of the fast multipole method without multipoles. *SIAM J. Sci. Stat. Comput.*, **13,** 923–947

Chorin, A. J. 1973. Numerical study of slightly viscous flow. *J. Fluid Mech.*, **57,** 785–796

Chorin, A. J. 1978. Vortex sheet approximation of boundary layers. *J. Comp. Phys.*, **27,** 428–442

Chorin, A. J. 1980. Vortex models and boundary layer instability. *SIAM J. Sci. Stat. Comput.*, **1,** 1–21

Chorin, A. J. 1994. Vorticity and turbulence. *Appl. Math. Sci.*, **103,**

Cooper, D., Jackson, D. C., Launder, B. E., and Liao, G. X. 1992. Impinging jet studies for turbulence model assessment—I. Flowfield experiments. *Int. J. Heat Mass Transfer*, **36,** 2675–2684

Craft, T. J., Graham, L. J. W., and Launder, B. E. 1992. Impinging jet studies for turbulence model assessment—II. An examination of the performance of four turbulence models. *Int. J. Heat Mass Transfer*, **36,** 2685–2697

Didden, N. and Ho, C. M. 1985. Unsteady separation in a boundary layer produced by an impinging jet. *J. Fluid Mech.*, **160,** 235–256

Greengard, L. and Rokhlin, V. 1987. A fast algorithm for particle simulations. *J. Comp. Phys.*, **73,** 325–343

Harvey, J. K. and Perry, F. J. 1971. Flowfield produced by trailing vortices in the vicinity of the ground. *AIAA J.*, **9,** 1659–1660

Hockney, R. W. and Eastwood, J. W. 1981. *Computer Simulations using Particles*, McGraw-Hill, New York

Launder, B. E. 1989. Second-moment closure: Present ... and future? *Int. J. Heat Fluid Flow*, **10,** 282

Peridier, V. J., Smith, F. T., and Walker, J. D. A. 1991. Vortex-induced boundary-layer separation. The unsteady problem $\mathrm{Re} \to \infty$. *J. Fluid Mech.*, **232,** 99–131

Puckett, E. G. 1991. The random vortex method with vorticity creation: Introduction and guide to parameter selection. *Lectures Appl. Math.*, **28,** 567–584

Saad, N. R., Polat, S., and Douglas, J. M. 1992. Confined multiple impinging slot jets without crossflow effects. *Int. J. Heat Fluid Flow*, **13,** 2–14

Sethian, J. A., Brunet, J. P., Greenberg, A., and Mesirov, J. P. 1992. Two-dimensional, viscous, incompressible flow in complex geometries on a massively parallel processor. *J. Comput. Physics*, **101,** 185–206

Strickland, J. H., Kempka, S. N., and Wolfe, W. P. 1995. Viscouse diffusion of vorticity using the diffusion velocity concept. *Proc. 2nd Int. Workshop on Vortex Flows and Related Numerical Methods*, Montreal, Canada, August 20–24

Strickland, J. H. and Baty, R. S. 1995. An overview of fast multipole methods. Sandia rep. SAND95-2405, UC-706, 39 pages

Walker, J. D. A., Smith, C. R., Cerra, A. W. and Doligalski, T. L. 1987. The impact of a vortex ring on a wall. *J. Fluid Mech.*, **181,** 99–140